The second-generation NIST standard hygrometer

C W Meyer[1,3]**, J T Hodges**[1]**, R W Hyland**[1]**, G E Scace**[1]**,
J Valencia-Rodriguez**[2] **and J R Whetstone**[1]

[1] National Institute of Standards and Technology, Gaithersburg, MD 20899, USA
[2] Advanced Scientific Applications de México, Puebla, Pue, Mexico

E-mail: christopher.meyer@nist.gov

Abstract
A second-generation standard hygrometer has been completed at the National Institute of
Standards and Technology (NIST). This hygrometer measures humidity using a gravimetric
method: it separates the water from the carrier gas and afterwards measures the water mass and
carrier gas mass. These two measurements determine the mass ratio r (the ratio of the
measured water mass to the measured dry-gas mass). The new design allows automated
continuous gas collection at up to $3 \, \text{L min}^{-1}$. This enables the hygrometer to collect larger
amounts of gas and thereby measure humidity values lower than that measured by the previous
NIST standard hygrometer. When operated in an optimal thermal environment (minimal
thermal loads in the laboratory), the total expanded relative uncertainty ($k = 2$) of the
gravimetric hygrometer is approximately 0.1% for atmospheric-pressure frost points higher
than $-35 \, ^\circ\text{C}$ ($r = 250 \, \mu\text{g g}^{-1}$). Below this frost point the total expanded relative uncertainty
gradually increases to approximately 1% at $-55 \, ^\circ\text{C}$ ($r = 13 \, \mu\text{g g}^{-1}$). The hygrometer has
measured the humidity of gas samples produced by the NIST Hybrid Generator and the NIST
Low Frost-Point Generator with dew/frost points from $-35 \, ^\circ\text{C}$ to $71 \, ^\circ\text{C}$. For both generators
the differences between the humidity generated and the humidity measured by the gravimetric
hygrometer are less than the combined uncertainties of the generator and the hygrometer.

(Some figures in this article are in colour only in the electronic version)

1. Introduction

The National Institute of Standards and Technology (NIST)
calibrates hygrometers using thermodynamic generators as
humidity sources. The two sources currently used are
the Hybrid Humidity Generator (HHG) [1, 2] and the
Low Frost-Point Generator [3], which produce atmospheric-
pressure dew/frost points of $-70 \, ^\circ\text{C}$ to $84 \, ^\circ\text{C}$ and $-100 \, ^\circ\text{C}$
to $-5 \, ^\circ\text{C}$, respectively. While these generators both have
solid thermodynamic foundations and well-characterized
uncertainties [2, 3], NIST considers it important to use
a primary gravimetric hygrometer [4] to validate the
performance of the generators. This hygrometer measures the
mass ratio r defined by

$$r \equiv m_{\text{w}}/m_{\text{g}} \qquad (1)$$

where m_{w} is the mass of the water in the gas and m_{g} is the
mass of the dry gas. The gravimetric hygrometer separates the
water from the gas, enabling mass measurement of each.

The technique of gravimetric hygrometry has been known
for over a century [4, 5], but it has not been widely used because
of its cumbersome nature and because it often takes a long
period of time to collect enough water to make an accurate
measurement. Gravimetric hygrometers are generally found
only in national standards laboratories [6, 7]. Even in these
laboratories, the use of gravimetric hygrometers is confined to
the validation or calibration of the humidity generators used to
calibrate customer hygrometers.

The first gravimetric hygrometer at NIST was developed
in 1948 by Wexler [8] in order to check the accuracy of
precision humidity generators. In 1963 Wexler and Hyland [9]
built a more sophisticated gravimetric hygrometer to be used
as the standard hygrometer for NIST, and it was used until
1988. Although measurements of r with this hygrometer had

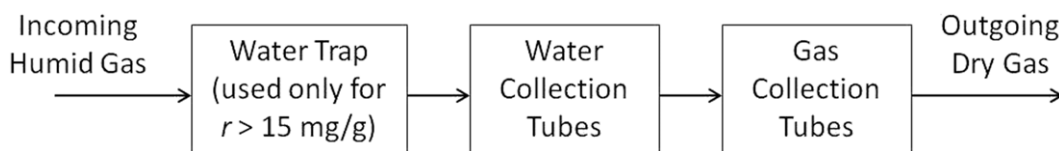[3] Author to whom any correspondence should be addressed.

Figure 1. Block diagram of the NIST gravimetric hygrometer.

a low expanded ($k = 2$) relative uncertainty of 0.13%, the gas-collection process was neither automated nor continuous, requiring relatively long times for thermal equilibrium at each step. In addition, the design of the water absorption system limited the collectible amount of water to about 0.5 g at average flow rates of the order of $1.5\,L\,min^{-1}$ (maximum, $2\,L\,min^{-1}$) before there was a significant likelihood of water loss. Operator endurance restricted the amount of time a humidity measurement could be made. The combination of all the above factors limited the range of the hygrometer to values above $190\,\mu g\,g^{-1}$. Operation of this hygrometer was an onerous experience and so it was used infrequently. As a result, plans were developed for a second-generation standard hygrometer that would expand the hygrometer's range and would enable more frequent use of the hygrometer.

In this paper we present a complete description of the design and operation of the second-generation NIST standard hygrometer. In sections 2 and 3, we describe the design and operation of the hygrometer, respectively. In section 4, we discuss the uncertainty budget for the hygrometer and plot the total uncertainty as a function of r. Finally, in section 5 we present comparisons between the hygrometer and the NIST HHG for a number of different values of r over a broad range and discuss the results.

2. Hygrometer design

The new gravimetric hygrometer employs water-collection tubes and an automated, continuous-flow gas-collection system. The design allows gas collection to be limited only by the patience of the operator. As the gas flows through the gravimetric hygrometer, desiccant-filled water-collection tubes trap the water in the gas before the gas enters the gas-collection system. For gas with mass ratios greater than $15\,mg\,g^{-1}$, the gas first flows through an additional water trap that condenses out most of the water and the rest is trapped by the desiccant. A block diagram of this system is shown in figure 1. The mass of the water is determined from the increase in mass of the water-collection tubes and trap (if used). The mass of the dry gas is determined by measuring the volume and density of the gas that has filled a gas-collection tube.

2.1. The water-collection system

2.1.1. Small mass ratios ($r \leqslant 15\,mg\,g^{-1}$). For mass ratios of $r \leqslant 15\,mg\,g^{-1}$, the water-collection system consists of three desiccant-filled tubes connected in series. A diagram of one of these tubes is shown in figure 2. Each tube is made of aluminium and plated with electroless nickel to prevent corrosion. It has an inner diameter of 2.22 cm and an outer

diameter of 2.54 cm. The tube has custom-designed flanges soldered to its ends, allowing them to be connected to the hygrometer manifold and sealed with Viton o-rings[4]. The flange design also allows caps to be placed on the top and bottom of the tube. These caps are also made of aluminium plated with electroless nickel. The length of the interior of the cap-sealed tube is 20.7 cm. The caps are sealed through Viton o-ring compression using a custom-made sealing tool which can turn and lift/lower a stainless-steel horizontal rod attached to the cap. The ends of this rod are positioned inside a slot in the flange (see figure) so that the compression increases as the rod is turned clockwise; once the rod reaches the end of the slot, the compression is sufficient to provide an airtight seal to the tube. When the rod is turned counterclockwise and lifted up, the cap is removed from the tube. Sealing/removal of the caps can be accomplished while the tube is either connected or disconnected to the manifold. To allow cap sealing/removal while connected to the manifold, sealing tools are mounted in the fittings above and below the tube in the manifold, as shown in figure 3.

Filter sheet of pore size 4 µm is used to keep the desiccant from escaping the water-collection tubes as gas passes through them. This sheet is attached with epoxy to the smaller end of rubber stoppers with 3 mm holes drilled through their axes. Two of these stoppers rest snugly inside the tube, one near each end, with the larger diameter side facing outwards. As additional protection, a small wad of quartz wool is placed between the desiccant and filter.

The first and second tubes that the gas passes through contain anhydrous $Mg(ClO_4)_2$ and the third tube contains anhydrous P_2O_5. The latter desiccant is more powerful, but the former is recyclable and more convenient to use. The first tube collects the vast majority of the water and the second tube collects the remaining amount. The third tube exists to verify that all water in the gas has been removed.

The unfilled water-collection tubes (including rubber stopper and quartz wool) weigh approximately 149 g. The packing of the tubes with desiccant is loose to ensure uniform gas flow through them and to prevent excessive flow impedance. The $Mg(ClO_4)_2$-filled tubes have an approximate mass of 179 g and the P_2O_5-filled tube has an approximate mass of 157 g.

2.1.2. Large mass ratios ($r > 15\,mg\,g^{-1}$). When the mass ratio is large ($r > 15\,mg\,g^{-1}$) the dew-point temperature of the

---

[4] In order to describe materials and experimental procedures adequately, it is occasionally necessary to identify commercial products by manufacturer's name or label. In no instance does such identification imply endorsement by the National Institute of Standards and Technology nor does it imply that the particular product or equipment is necessarily the best available for the purpose.
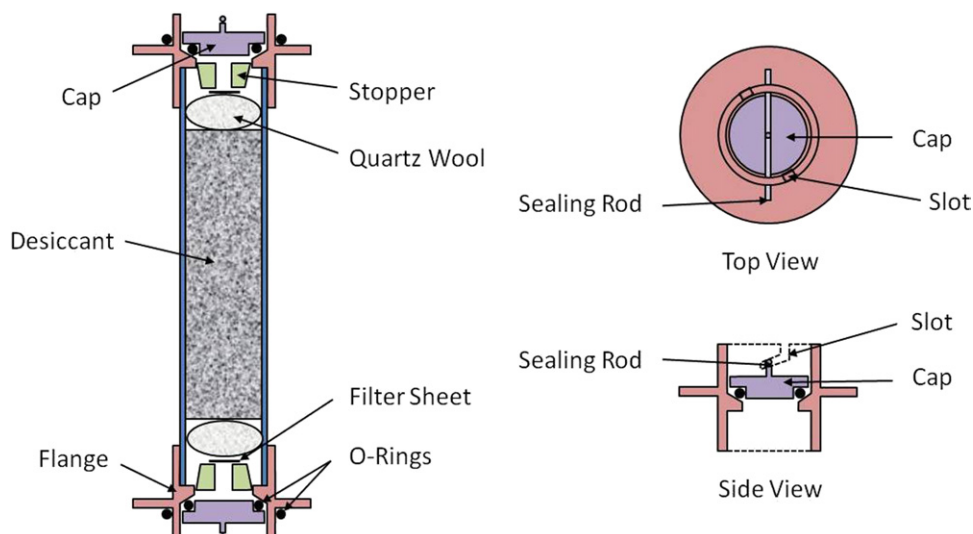
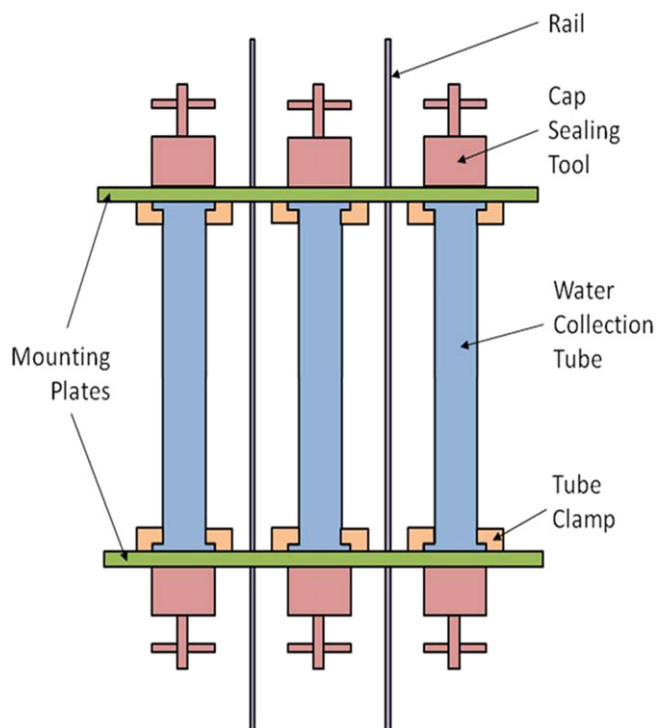**Figure 2.** Diagram of water-collection tubes, including details of the cap-sealing rod and flange slot.

Figure 3. Mounting of water-collection tubes in the manifold of the gravimetric hygrometer.

Figure 4. Water trap for the gravimetric hygrometer, which is used when the dew-point temperature of the gas is above the ambient temperature.

entering gas is near or above the ambient temperature, allowing undesired water condensation in the manifold of the system described in section 2.1.1. To prevent this, an additional water trap is added that ensures the dew point of the gas entering the manifold is below ambient temperature. When measuring the water mass collected by the gravimetric hygrometer, the mass of water collected in this trap is included.

The trap, shown in figure 4, consists of two concentric stainless-steel cylindrical containers that are joined together at the top by a stainless-steel annular plate; this plate is welded to the tops of both containers to make a single sealed container with a well, as shown. The container has a diameter of
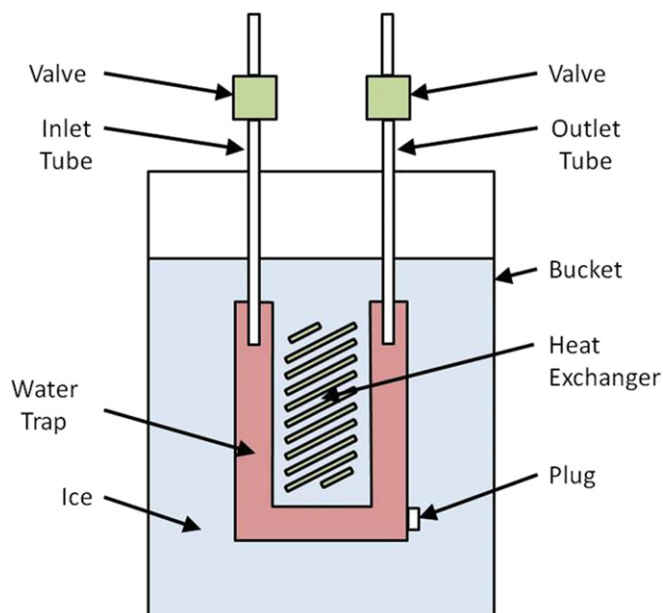
12.3 cm and a height of 17.3 cm. The well of the container has a diameter of 8.4 cm and a depth of 10.5 cm. With these dimensions the trap can hold up to approximately 1450 cm^3 of water. Two 1 cm diameter stainless-steel tubes are used as inlet and outlet tubes; they are welded into two holes that were drilled at opposite sides in the plate. Valves are attached to the tops of the tubes to seal the trap when desired. Drainage of the water from the trap is accomplished by opening a stainless-steel plug sealed with an o-ring.

Immediately before operation of the gravimetric hygrometer, the trap is placed in a large bucket. A heat exchanger consisting of coiled copper tubes is placed in the well of the trap, as shown; cold water (1 °C) is circulated through these tubes. Afterwards, the bucket is filled with ice to a point above

the top of the trap but underneath the valves, as shown in the figure. The inlet valve and the tubing leading to it are heated to approximately $10\,^\circ$C above the dew-point temperature of the gas in order to prevent water condensation in them.

To validate the performance of this trap, control tests were performed in which a chilled-mirror hygrometer was attached to the outlet of the trap. The hygrometer measured dew-point temperatures that were less than $10\,^\circ$C, even when the dew point of the incoming gas was $85\,^\circ$C.

2.2. Water mass measurement

2.2.1. Collection-tube mass determination. The mass of each tube is determined using a commercial electronic balance. The closed chamber of the balance has been modified to accommodate the size of the tubes. The metal composition of the tubes ensures no electrostatic buildup on the tubes as they are being weighed (which can cause measurement errors). In order to minimize uncertainties caused by drift of the balance, the mass of each tube is determined by comparing its mass against that of a corresponding standard mass. Because only the change in mass of the tubes (after water collection) is relevant, no high-accuracy calibrations of the standard masses have been performed; periodic mass measurements of the mass standards using the balance are deemed sufficient. The first and second tubes are compared against a 179 g standard mass. The third tube is compared against a 157 g standard mass. A sensitivity mass of 2 g is used in the comparison measurements to make mass comparison uncertainties less dependent on electronic balance uncertainties.

Before performing mass comparison measurements, the flange o-rings are removed from the tubes and the tubes are left inside the balance chamber. The apparent mass of the first tube is measured and monitored as a function of time using a computer. The monitoring continues until the measured mass is observed to be constant (typically 90–120 min); this ensures that thermal equilibrium has been reached and that no convective air currents distort the mass measurements. If the operating gas is air, then immediately before the measurements, one cap of each tube is removed for approximately 1 s and then resealed to ensure that the air inside the tubes is at ambient pressure.

At the beginning of a collection of measurements, the ambient pressure is measured with an aneroid barometer in the room, the temperature is measured by an industrial platinum resistance thermometer placed inside the balance chamber and the relative humidity is measured by a commercial polymer-film capacitance hygrometer. All objects are placed on the balance with tongs to minimize thermal exchange. To maximize measurement reproducibility, a specially designed aluminium ring has been placed on the balance tray to centre both tubes and standard masses when being weighed. Each mass value is transferred to a computer and recorded in a spreadsheet. Measurements are made every 5 s for 40 s, and the last four measurements are used to calculate an average value. Each measurement is plotted in real time to allow the operator to verify that a steady state has been reached. For one mass comparison measurement set, each tube is placed sequentially

on the balance and its mass is recorded. Afterwards, similar measurements are made for the standard mass and then the combination of standard mass and sensitivity mass. This set of comparison measurements is repeated three times. At the end of the collection of measurement sets, the pressure and temperature are once more recorded to check for drift. The repeatability of a mass measurement is typically $70\,\mu$g.

Each tube mass is calculated with the single-substitution method using the following equation:

$$
\begin{aligned}
m_\mathrm{t} = m_\mathrm{s} + \rho_\mathrm{a}(V_\mathrm{t} - V_\mathrm{s}) + \left(m'_\mathrm{t} - m'_\mathrm{s}\right) \\
\times (m_\mathrm{sens} - \rho_\mathrm{a} V_\mathrm{sens})/m'_\mathrm{sens},
\end{aligned}
\tag{2}
$$

where m_t is the real mass of the tube, m_s is the real mass of the standard, m_sens is the real mass of the sensitivity standard and m'_t is the measured mass of the tube, m'_s is the measured mass of the standard and m'_sens is the measured mass of the sensitivity standard. The value of m'_sens is determined by $m'_\mathrm{sens} = m'_\mathrm{com} - m'_\mathrm{s}$, where m'_com is the measured mass of the combination of standard mass and sensitivity mass. The second term on the r.h.s. of equation (2) is the buoyancy correction, where V_t is the volume of the tube and V_s is the volume of the standard mass. The tube volume is $(125 \pm 1)\,\mathrm{cm}^3$, a value determined by immersing the empty tube (with caps on) in a graduated cylinder filled with water. The volume of the standard is calculated by dividing the mass of the standard by the density of stainless steel ($7.84\,\mathrm{g\,cm}^{-3}$). In the buoyancy correction, ρ_a is the density of moist air at the measured temperature, pressure and relative humidity, as determined by the CIPM-2007 formula [10]. The third term on the r.h.s. of equation (2) is the difference between the measured mass of the tube and that of the standard, with corrections based on the difference between the measured value of the sensitivity mass and its true value. Here, V_sens is the volume of the sensitivity mass.

2.2.2. Correction for the mass of the gas in the water-collection tubes. Because a water-collection tube contains gas as well as solid materials, we account for changes in the gas mass when calculating the collected mass of water from the measured change in collection-tube mass. The mass of the water collected is then

$$
m_\mathrm{w} = m_\mathrm{t}^\mathrm{f} - m_\mathrm{t}^\mathrm{i} - \Delta m_\mathrm{tg} = m_\mathrm{t}^\mathrm{f} - m_\mathrm{t}^\mathrm{i} - \left(V_\mathrm{tg}^\mathrm{f}\rho_\mathrm{tg}^\mathrm{f} - V_\mathrm{tg}^\mathrm{i}\rho_\mathrm{tg}^\mathrm{i}\right), \tag{3}
$$

where m_t^i and m_t^f are the initial and final masses of the tube as determined by equation (2), respectively, and Δm_tg is the change of the gas mass in the tube. The values V_tg^i and V_tg^f are the initial and final volumes of gas in the tube, respectively, and $\rho_\mathrm{tg}^\mathrm{i}$ and $\rho_\mathrm{tg}^\mathrm{f}$ are the initial and final gas densities in the tube, respectively.

We obtain the gas volume in each collection tube, V_tg, using the known value of the original gas volume inside that tube (before any water has been collected), V_tg^o. For the first tube, a correction is made to this volume to account for the decrease in gas volume due to the increase in desiccant volume resulting from water absorption. As water is absorbed by $\mathrm{Mg(ClO_4)_2}$, the increase in desiccant volume is due to the processes

$$
\mathrm{Mg(ClO_4)_2} + n\mathrm{H_2O} \rightarrow \mathrm{Mg(ClO_4)_2} \cdot n\mathrm{H_2O}, \tag{4}
$$

where $n = 2, 4$ or 6 [9]. Assuming equal reaction distributions, Wexler and Hyland have shown that the reactions result in desiccant volume increases of $(0.819 \pm 0.057) \, cm^3$ per gram of H_2O absorbed [9]. The gas volume is then

$$V_{tg} = V_{tg}^o - 0.819 \, cm^3 \, g^{-1} \cdot m_w^{tot}, \quad (5)$$

where m_w^{tot} is the total amount of water absorbed in the collection tube since it was filled with fresh desiccant. For every $2 \, g$ H_2O absorbed in the desiccant, the decrease in the gas mass due to such a volume change would be $\approx 1.5 \, mg$ or 0.08%. We do not make this correction for the second and third tubes because the water absorbed in them is small.

We measured the value of V_g^o for each collection tube and we assume it to be the same value each time the tube is refilled. It was measured using the gas-collection system (described in section 2.3) in the following manner. We first filled the collection tubes with a fresh sample of dry desiccant. The manifold, including the water-collection tubes, was then filled with N_2 to twice the ambient pressure, as measured by a Bourdon gauge, and sealed using the appropriate valves. We subsequently closed the caps to all collection tubes, keeping this pressure inside the tubes. The manifold was reduced to ambient pressure by opening and then closing a valve. We then opened the caps to one of the collection tubes, raising the pressure in the manifold. Finally, the gas-collection system was opened to the manifold so that the pressure in the manifold dropped to ambient pressure as the collection system collected the excess volume of gas (equal to the volume of gas in the water-collection tube). We performed this procedure to all three water-collection tubes.

The empty collection tubes (with no rubber stoppers or quartz wool inside) were determined through dimensional measurements to have a volume of $(80 \pm 1) \, cm^3$ and measurements using the gas-collection procedure described above yielded $(80 \pm 2) \, cm^3$. When we filled tubes 1 and 2 with dry $Mg(ClO_4)_2$ and placed the stoppers and quartz wool inside, we measured the gas volume to be $(55 \pm 2) \, cm^3$. When tube 3 was filled with dry P_2O_5 and the stoppers and quartz wool were placed inside, the gas volume in each of these tubes was measured to be $(61 \pm 2) \, cm^3$.

Changes in gas density are usually due to changes in gas temperature and pressure in the collection tube, but they can also occur due to a change in gas composition if the operating gas is different than air. We have elected to prevent gas composition changes by placing the collection tubes in the manifold and flushing them with the operating gas before making the initial tube mass measurements. To account for density changes in equation (3), temperature and pressure measurements are made of the gas before the collection-tube caps are closed. We make these measurements using the gas-collection system described in section 2.3.

2.2.3. Capacity of the first water-collection tube. It is important to know the maximum amount of water that can be trapped in the first water-collection tube before significant amounts of water escape it. We determined this by measuring
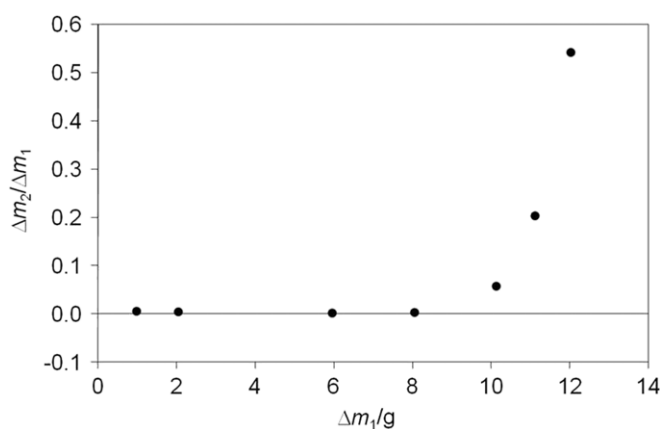

Figure 5. Ratio of water collected in the second collection tube Δm_2 to that in the first tube Δm_1 as a function of Δm_1.

the ratio of water collected in the second collection tube Δm_2 to that in the first tube Δm_1 as a function of Δm_1. Humid gas was passed through the gravimetric hygrometer with a flow rate of $3 \, L \, min^{-1}$ for short periods of time, after which the collection tubes were removed from the manifold, weighed and replaced on the manifold. We then repeated the process a number of times. The results of this test are shown in figure 5. The ratio $\Delta m_2 / \Delta m_1$ is below 0.01 for $\Delta m_1 \leqslant 8 \, g$. For values of Δm_1 larger than this, $\Delta m_2 / \Delta m_1$ is prohibitively large to provide high confidence that all water is trapped in the collection tubes. A water collection of $8 \, g$ is sufficient to make uncertainties due to collection-tube gas mass changes acceptably small.

2.2.4. Water escaping the collection tubes. When operating the gravimetric hygrometer, we assume that all the water in the gas passing through the water-collection tubes is trapped by the desiccant. We tested this assumption in an experiment where moist N_2 with a dew-point temperature of $T_{DP} \approx 18 \, °C$ was passed through the collection tubes. The residual humidity in the gas (measured as frost-point temperature T_{FP}) was then measured with a commercial chilled-mirror hygrometer. We placed a filter between the collection tubes and the hygrometer to ensure that no desiccant particulates would enter the hygrometer. The flow rates ranged from $0.5 \, L \, min^{-1}$ to $3 \, L \, min^{-1}$. The resulting value of T_{FP} varied from $-100 \, °C$ to $-86 \, °C$ and we found it to be independent of flow rate over the range used. An example of this is shown in figure 6, where the flow rate is $2 \, L \, min^{-1}$. It is likely that the large variation observed in the measured moisture is due to absorption/desorption of water in the filter between collection tubes and hygrometer. We also measured similar values of T_{FP} when dry gas evaporating from a liquid N_2 dewar was passed through the collection tubes. From these control tests, we estimate the upper limit for moisture escaping the water-collection tubes to be $T_{FP} = -86 \, °C$ (a mass ratio of $0.13 \, μg \, g^{-1}$). From this upper limit we estimate the gravimetric hygrometer's standard uncertainty component due to moisture escape to be $u(r) = 7.5 \times 10^{-2} \, μg \, g^{-1}$. This corresponds to an uncertainty in the mass of the water escaping the collection tubes of $u(m_{esc}) = 7.5 \times 10^{-8} m_g$.
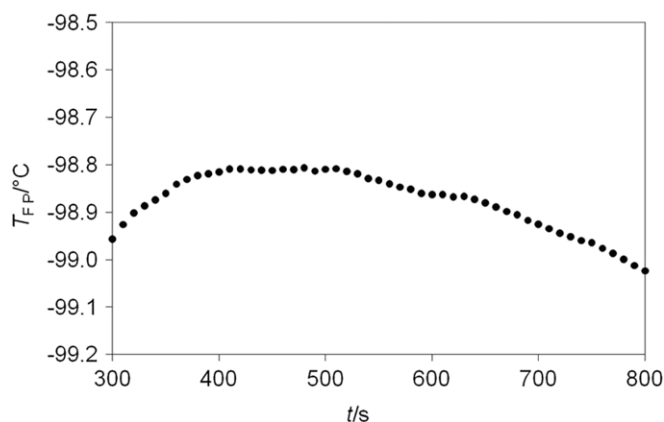
Figure 6. Residual frost-point temperature T_{FP} of N_2 gas as a function of time t after passing through water-collection tubes. The measurement of T_{FP} was made with a chilled-mirror hygrometer. The dew-point temperature of the gas before going through the collection tubes was $T_{DP} \approx 18\,°C$.

2.2.5. Water-trap mass determination.

We use a commercial electronic balance to determine the mass of the trap. The balance is a different model than that used for the collection tubes, and is capable of mass measurements of up to 10 kg. No chamber encloses the trap while mass measurements are being made. Before performing the mass comparison measurements, we place the trap next to the balance and leave it for at least 14 h to reach thermal equilibrium. Immediately before the measurements, we briefly open one of the trap valves and then close it to ensure that the gas inside the trap is at ambient pressure. If the operating gas is not air, we still use this step because the opening of the valve always results in gas expulsion from the trap. (This is the case because the gas flows through the trap while it is at approximately 0 °C.)

We determine the mass of the trap by comparing its mass against that of a 1350 g standard mass. A sensitivity mass of 100 g is used. At the beginning of a collection of measurements, we measure the ambient pressure with an aneroid barometer, the temperature with an industrial platinum resistance thermometer placed near the balance and the relative humidity with a commercial polymer-film capacitance hygrometer. Each mass value measured with the electronic balance is automatically transferred to a computer, where it is recorded in a spreadsheet. The measurement protocol is identical to that for the water-collection tubes as described in section 2.2.1. With the balance and weighing technique used, the repeatability of a mass measurement is typically 2 mg. We calculate the mass of the trap using equation (2) and the calculation methods described in section 2.2.1, where the volume of the trap is $(1600 \pm 20)\,cm^3$. We determined this value for the volume by dimensional measurements of the container and inlet/outlet tubes and by immersing the valves in a graduated cylinder filled with water.

As before, changes in gas mass must be accounted for when calculating the collected mass of water from the measured change in water-trap mass. The mass of the water collected is given by equation (3). In the equation, V_{tg}^f is given by

$$V_{tg}^f = V_{tg}^i - m_w \rho_w \cong V_{tg}^i - \left(m_t^f - m_t^i\right)\rho_w, \tag{6}$$

where now m_t^i and m_t^f are the initial and final masses of the water trap, respectively, and ρ_w is the density of water. We assign the value of V_{tg}^i to be $1450\,cm^3$ when the trap has no water inside. If the trap has water inside from a previous use, we assign V_{tg}^i the value of V_{tg}^f from the last measurement.

2.3. The dry-gas collection system

2.3.1. Prover tubes.

The centrepiece of the dry-gas collection system is a pair of precision-bore glass vertical cylinders (prover tubes) of length 0.927 m and diameter 0.1437 m. Teflon[4] pistons are located inside them, as shown in figure 7. The bottom of the prover tubes is closed by a Delrin[4] cap. The cap contains a groove in which a Viton o-ring[4] is seated, providing an airtight seal. The cross-sectional areas of these prover tubes were measured by the NIST machine shop using a coordinate measuring machine. The measured areas A were fitted using a fourth-order polynomial function:

$$A = \sum_{i=0}^{4} a_i z^i, \tag{7}$$

where z is the vertical distance from the bottom of the tubes and the coefficients a_i are the polynomial coefficients.

The areas were determined to be uniform over their length to within $4 \times 10^{-2}\,cm^2$. The diameters of the pistons are $2 \times 10^{-3}\,cm$ smaller than that of the prover tubes. Mercury 'o-rings' of diameter 0.4 cm provide an airtight seal between the pistons and cylinders, yet still allow the pistons to move vertically. The o-rings hold together by the surface tension of the mercury. As each piston moves along its cylinder, the mercury rotates about its axis to maintain the seal.

For each prover tube, a computer-automated laser interferometry system measures the position of the piston relative to its starting position with an uncertainty of $1.6 \times 10^{-7}\,m$. As a prover-tube collects gas, the piston rises
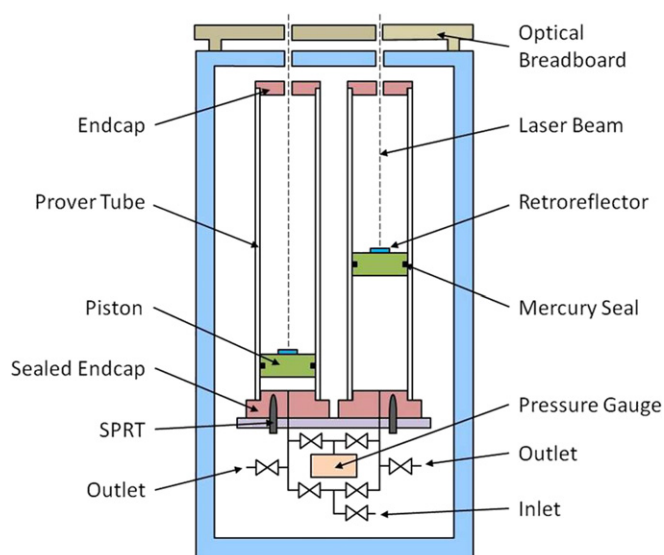

Figure 7. The dry-gas collection system, comprising two glass cylindrical tubes with Teflon pistons inside. Mercury o-rings seal the pistons against the tubes but allow vertical motion of the pistons.
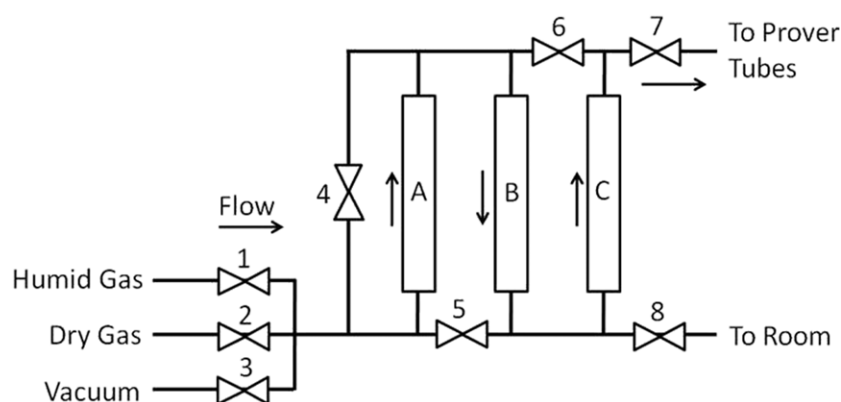
Figure 8. Manifold for the water-collection tubes. When the water trap is used, the outlet from the trap connects to the 'humid gas' inlet. The valves are labelled by numbers and the water-collection tubes are labelled by letters. The arrows represent the gas flow directions during the water collection.

from its initial position until it reaches a final position ~60 cm higher, at which point the volume of gas collected between the initial position and final position ($\approx$9.4 L) is calculated. Pressure and temperature measurements are then performed to determine the density of gas, which along with the volume yields the mass of the gas collected by the prover tube. Subsequently the gas is purged from the prover tubes by opening a pneumatic valve to the room and allowing the piston to fall to its initial position, allowing another collection of gas at a later time.

2.3.2. The manifold. The manifold connects the incoming gas to the water trap (if used), water-collection tubes and dry-gas collection system. The tubes of the manifold are made of electro-polished stainless steel to ensure cleanliness and minimal water adsorption on the tube walls. During normal gas/water collection the gas is directed sequentially through the water trap (if used) and water-collection tubes and then through the dry-gas collection system. A filter is placed between the last water-collection tube and the dry-gas collection system to ensure that no desiccant powder is able to enter the system. For special circumstances, the water-collection tubes can be bypassed by closing their caps and opening certain valves on the manifold, allowing the moist gas to go directly to the prover tubes.

The manifold has been specially constructed to allow convenient insertion and removal of the water-collection tubes. To accomplish this, the tubes are located between two horizontal platforms which are attached to the manifold mounting, as shown in figure 3. The top platform can be moved vertically by sliding along two vertical guiding rods mounted on the bottom platform. Holes in the top and bottom platforms allow insertion of the tops and bottoms of the water-collection tubes, and o-rings on the tube flanges seal the tubes to the platforms. Special connectors are mounted on the other side of these holes to allow connection of the water-collection tubes to the manifold. Flexible bellows tubes connect the top platform connectors to the rest of the manifold, allowing movement of the top platform for insertion and removal of the water-collection tubes.

The manifold for the water-collection tubes is shown in figure 8. When no water trap is used, the humid gas enters the manifold as shown. When the water trap is used, the outlet from the trap is attached to the 'humid gas' inlet. The manifold features a connection to a dry-gas supply and a connection to a roughing pump that provides a vacuum. The dry-gas supply and pump are separated from the water-collection tubes by valves. They are present to allow drying out the manifold before opening the tubes and operating the hygrometer. The drying is accomplished by first closing valves 1, 7 and 8, opening valves 4–6 and performing a series of three pump-and-purge cycles. In each cycle (1) the manifold is pumped out until an adequate vacuum is achieved (as shown by a thermocouple gauge) and (2) dry gas (120 kPa) is introduced into the manifold. After three cycles, valve 8 is opened briefly to lower the gas pressure in the manifold to ambient. The hygrometer is operated with valves 1 and 7 opened, valves 2–6 and 8 closed and all tube caps opened.

2.3.3. Dead-space volumes. When the water trap is used, a dead space of $\approx$30 cm^3 exists between the water trap and the first water-collection tube. At the end of each use of the gravimetric hygrometer, gas with a dew-point temperature of approximately 10 °C will stay in this space and will not be collected by the water-collection tubes. However, when the water trap is used, the water collected by the entire water-collection system is at least 25 g, and the mass of water in the dead space is approximately 2 mg, which may be considered negligible.

There are two additional dead space volumes, one for each prover tube. These are the volumes between the bottom of each prover piston at its lowest position and the valve separating the manifold from the prover tubes. It is necessary to know the values of these prover-tube dead space volumes for proper accounting of the gas mass collected. For the portion of the dead space involving the admission and exhaust valves, the information provided in the valve specifications was used to obtain the valve's contribution to the volume. The rest of the dead space volume was determined by geometric calculation and, when possible, measurement of the water volume that could be contained inside the space. The dead space volume under the left piston was determined to be $1.191\,416 \times 10^{-3}$ m^3 and that under the right piston was

determined to be $1.191\,349 \times 10^{-3}\,\text{m}^3$, where the standard uncertainty ($k = 1$) of the volumes was $1 \times 10^{-6}\,\text{m}^3$. The dead space volumes are relevant for the dry-gas collection because of possible pressure changes from the beginning of the gas-collection cycle (piston at the bottom of prover tube) to the end (piston at top). These pressure changes lead to changes in the mass of the gas in the prover tube's dead space, which must be accounted for. The procedure for accounting for these mass changes is given in section 2.3.7.

2.3.4. Automation for continuous gas flow. The computer coordinates the gas collection of both prover tubes so that gas is collected by the system at a steady rate. It accomplishes this by opening up the gas flow to one prover tube once the other tube has reached a position close to its final position. After a brief period while both tubes collect gas, the valve to the filled prover tube is closed and all gas collection is performed by the other tube. As the pressure measurements are made in the filled tube and the gas is purged, the collection continues in the other tube. This data collection technique allows a maximum of $4\,\text{L}\,\text{min}^{-1}$ for the rate of gas flow through the gravimetric hygrometer.

2.3.5. Gas volume measurement. The gas-collection system employs a Hewlett Packard (Agilent) 5501A laser transducer[4] to determine the prover piston displacement. This consists of a frequency-stabilized He–Ne laser which has a vacuum wavelength of $\lambda_\text{o} = (632.991\,37 \pm 0.000\,12)\,\text{nm}$. The apparent wavelength λ is obtained by dividing λ_o by the index of refraction of air n. The value of n is determined using the formula of Ciddor [11]. For determining n, the room temperature is assumed to be 20 °C, the relative humidity is assumed to be 50% and the ambient pressure is measured by a piezoresistive transducer; this yields a standard uncertainty for n of 1×10^{-6}. The laser uses the Zeeman effect (by way of a magnet surrounding the laser tube) so that the laser beam has two orthogonal polarizations that have slightly different frequencies f_1 and f_2. The laser is mounted on an optical breadboard positioned over the two prover tubes. A beamsplitter separates the laser light into two horizontal beams, one for each tube. A set of adjustable mirrors directs each laser beam to a mirror situated immediately above the corresponding prover tube. For each tube, this top mirror directs the beam vertically down along the axis of the prover tube. An optically separating beamsplitter beneath the top mirror reflects the part of the beam with frequency f_2 coming from the top mirror to a side retroreflector that reflects the f_2 beam back to the beamsplitter. The part of the beam with frequency f_1 is transmitted through the beamsplitter to a retroreflector mirror on top of the piston in the prover tube. When the piston moves, the Doppler effect shifts the frequency of the f_1 beam to give it frequency $f_1 + \Delta f_1$, where the sign of Δf_1 depends on the direction of the piston movement. The f_1 beam is then recombined with the f_2 beam before reaching the photodetector. The signal from the photodetector has a modulation frequency of $f_2 - (f_1 + \Delta f_1)$. This signal is then compared with a reference signal coming from the laser with frequency $f_2 - f_1$. A pulse converter then uses these

signals to obtain Δf_1 and uses it to provide a pulse for every piston displacement equivalent to $\lambda/4$. Counting these pulses provides a method for measuring the total displacement of the piston with a resolution of $1.6 \times 10^{-7}\,\text{m}$ as it collects dry gas.

The volume of gas collected in the prover tube by the displaced piston, V_p, is then

$$V_\text{p} = \int_{z_1}^{z_2} A(z)\,\text{d}z. \tag{8}$$

Here, z_1 is the vertical position of the piston at the beginning of the cycle (bottom of prover tube), z_2 is the vertical position of the piston at the end of the cycle (top of prover tube) and $A(z)$ is the area of the prover tube at vertical position z.

2.3.6. Gas density determination. The pressure underneath the piston inside both prover tubes is measured by a single commercial quartz Bourdon gauge. The Bourdon gauge is calibrated every six months by comparison with a piston gauge whose calibration is traceable to the NIST Pressure and Vacuum group. Its zero offset is measured every six months by measurement against a vacuum provided by a mechanical pump. The Bourdon gauge measures pressure with an estimated standard uncertainty of 13 Pa. Stainless-steel tubes connect the Bourdon gauge to both prover tubes. Two pneumatic valves controlled by the computer determine the prover tube whose pressure is to be measured. During a collection cycle the pressure is measured before gas collection begins and after gas collection ends. No correction is made to account for the aerostatic pressure head because the pressure difference between the bottom and the top is calculated to be less than 7 Pa, or less than 0.01% of the pressure measurement.

The temperature underneath the pistons in the prover tubes is measured by two standard platinum resistance thermometers (SPRTs). A current of 1 mA is passed through each SPRT and a standard resistor in series. For measuring the SPRT resistance, a multimeter measures the ratio of the voltage drop across the SPRT to the drop across the standard resistor. Reversing the current, repeating the measurement and averaging both ratios cancels stray thermal emfs. The SPRTs are mounted in the caps at the bottom of the tubes so that their tops protrude into the gas in the tubes. The SPRTs were calibrated by the NIST Thermometry Group over the range 0 °C to the melting point of gallium (29.7646 °C) with an expanded ($k = 2$) calibration uncertainty of 4×10^{-5} °C.

The gas density is calculated using the pressure and temperature measurements described above along with the virial equation of state. The virial coefficients for air have been obtained from Hyland and Wexler [12] and those for nitrogen have been obtained from McLinden and Losch-Will [13].

2.3.7. Mass of the collected gas. The total mass of gas collected for one cycle is

$$m_\text{g} = \rho_\text{f} V_\text{p} + (\rho_\text{f} - \rho_\text{i}) V_\text{d}, \tag{9}$$

where ρ_i is the density measured at the beginning of the collection cycle (piston at bottom of the prover tube), ρ_f is

the density measured at the end of the collection cycle (piston at top of the prover tube) and V_d is the type B dead space volume mentioned in section 2.3.3.

3. Hygrometer operation

If necessary, the water-collection tubes are refilled with desiccant and the water trap (if used) is emptied. The first water-collection tube is refilled with $Mg(ClO_4)_2$ if it is anticipated that the total water mass in the tube after water collection will exceed 8 g. The second and third tubes are refilled (with $Mg(ClO_4)_2$ for tube 2 and P_2O_5 for tube 3) if they have already collected 2 g of water; this occurs only rarely since these tubes generally collect less than 1% of that collected by the first tube. The refilling is done in a dry box to ensure minimal water absorption by the desiccants during the process. The first tube and second tube are filled until they weigh 179 g and the third tube is filled until it weighs 157 g.

Before weighing, the water-collection tubes and the water trap (if used) must be filled with the operating gas. If the operating gas is air, nothing is done because the tubes and trap already contain air. If the operating gas is not air, the water-collection tubes and water trap are first mounted in the manifold of the gravimetric hygrometer. Dry gas of the type of the test gas is flushed through the water-collection tubes and water trap and then the gas pressure is measured. The flushing is accomplished by opening the tube caps and passing a minimum of 200 L of gas through the hygrometer. A computer program automates the process, as in a normal gas collection. The flow is stopped by closing the inlet valve and waiting for the piston in the active prover tube to stop rising. The pressure and temperature inside the water-collection tubes and water trap are measured by assuming they are equal to their counterparts in the active prover tube. The remaining caps to the water-collection tubes are closed and the tubes removed from the manifold.

Once the tubes contain the proper gas and the pressure inside is known, the tubes are weighed as described in section 2.2. Afterwards they are remounted in the hygrometer manifold.

If the water trap is used, it is attached to the manifold as described in section 2.3.2. The trap is placed in a bucket, and the heat exchanger is placed in the well of the trap, as shown in figure 4. The bucket is filled to the top with ice cubes and afterwards with chilled water to fill in the gaps between the ice cubes. After the trap has reached thermal equilibrium with the ice, the outlet valve for the trap is opened and dry gas is introduced into the trap until it reaches ambient pressure.

If necessary, the manifold for the water-collection tubes is dried by the pump-and-purge process described in section 2.3.2. Tests using dry gas have shown that initial moisture in the manifold, if not removed, causes the collection-tube masses to increase by 2 mg to 3 mg during hygrometer operation. For measurement of small mass ratios, where only 2 g of water is gathered in the collection tubes, this is a significant amount; therefore, for this arrangement, the manifold is always dried.

The collection process is then started, automated through the computer program. Valves in the manifold are adjusted until a flow rate of $2 \, L \, min^{-1}$ to $3 \, L \, min^{-1}$ is obtained. Calculations are made to determine the amount of gas to collect in order to collect 2 g of water (low mass ratio measurements) or 50 g of water (high mass ratio measurements using the water trap). If necessary, less water may be collected due to time constraints. Once the desired amount of gas has been collected, the collection is ended by closing the inlet valve and waiting for the flow to stop, as before. The valves to the water trap (if used) are closed, the caps to the water-collection tubes are closed and the computer program is stopped.

The entrance gas segment and exit gas segment require special consideration because they have been through either water collection or gas collection but not both. They are associated with the section of the manifold between the last water-collection tube and the bottom of the active prover piston. The entrance/exit gas segments are located in this section at the beginning/end of the gas-collection process, respectively. While the entrance gas segment does not pass through any water-collection tubes, it is collected in the prover tubes. Similarly, while the exit gas segment passes through the water-collection tubes, the gas flow ends before it can be collected in the prover tubes. Uncertainties due to the existence of these gas segments can be minimized by (1) flushing out the manifold with dry gas before beginning collection of the test gas and (2) ensuring that the pressure and temperature in the manifold after the collection are approximately the same values as those before the collection. The latter item is accomplished by closing the downstream cap to the first water-collection tube to end the water collection and waiting until the pistons in the prover tubes stop rising before terminating the gas-collection process. If this is done, the number of moles of the two segments is approximately the same. They can then be treated in the analysis as one segment of gas that has gone through both the water collection and the dry-gas collection.

When the collection is over, the tubes and trap (if used) are once again removed from the manifold and reweighed. The mass changes for all the water-collection tubes and the trap are calculated and corrected for gas mass changes. Data evaluation is achieved by entering the acquired raw data into a spreadsheet template, which then calculates the total water mass collected, the total gas mass collected and the resulting mass ratio.

4. Uncertainty budget

The uncertainty analysis here complies with the ISO *Guide to the Expression of Uncertainty in Measurement* [14]. It assumes the measurement protocol described in the previous section.

The equation for the relative uncertainty $u(r)/r$ for the mass ratio measured by the gravimetric hygrometer is derived in the appendix. The equation is as follows:

$$\frac{u(r)^2}{r^2} = \frac{u(m_w)^2}{m_w^2} + \frac{u(m_g)^2}{m_g^2}. \tag{10}$$

Table 1. Uncertainty budget for the gravimetric hygrometer, in measurement units and in percentage of mass ratio r. Water mass-measurement uncertainties are given for low r (no water trap used) and for high r (water trap used). For the relative uncertainty values of the water mass-measurement components, it is assumed that 2 g (50 g) of water is collected for low r (high r). For the relative uncertainty values of the gas mass-measurement components, it is assumed that the temperature and pressure of the gas in the prover tubes are 20 °C and 101 325 Pa, respectively.

Description	x	$u(x)$	Contribution to $u(r)/r \times 100$
Water mass meas. ($r \leqslant 15$ mg g^{-1})			
Mass measurements	m'	7.0×10^{-5} g	1.5×10^{-2}
Sensitivity mass	m_{sens}	1.2×10^{-4} g	6.0×10^{-3}
Air pressure	P_{a}	25 Pa	4.0×10^{-3}
Air temperature	T_{a}	0.2 °C	1.0×10^{-2}
Air relative humidity	RH	1%	5.0×10^{-3}
Water escaping collection tubes	m_{esc}	$7.5 \times 10^{-8} m_{\text{g}}$	$7.5 \times 10^{-6}/r$
Water mass meas. ($r > 15$ mg g^{-1})			
Mass measurements	m'	2.0×10^{-3} g	0.9×10^{-2}
Sensitivity mass	m_{sens}	3.0×10^{-3} g	6.0×10^{-3}
Air pressure	P_{a}	25 Pa	1.1×10^{-3}
Air temperature	T_{a}	0.2 °C	2.8×10^{-3}
Air relative humidity	RH	1%	1.4×10^{-3}
Gas mass measurement			
Gas temperature	T_{g}	0.1 °C	3.4×10^{-2}
Gas pressure	P_{g}	13 Pa	1.3×10^{-2}
Prover tube piston displacement	Δz	4.7×10^{-3} cm	7.8×10^{-3}
Prover tube area	A	9.0×10^{-3} cm^2	5.5×10^{-3}

When only the three water-collection tubes are used,

$$\frac{u(m_{\text{w}})^2}{m_{\text{w}}^2} = \frac{10\rho_{\text{a}}^2 [V_{\text{t}} - V_{\text{s}}]^2}{m_{\text{w}}^2}$$
$$\times \left[\frac{u(P_{\text{a}})^2}{P_{\text{a}}^2} + \frac{u(T_{\text{a}})^2}{T_{\text{a}}^2} + \left(\frac{1}{\rho_{\text{a}}} \frac{d\rho_{\text{a}}}{d(\text{RH})} \right)^2 u(\text{RH})^2 \right]$$
$$+ \frac{17 u(m')^2}{m_{\text{w}}^2} + \frac{u(m_{\text{sens}})^2}{m_{\text{w}}^2} + \frac{u(m_{\text{esc}})^2}{m_{\text{w}}^2}, \quad (11)$$

where P_{a} and T_{a} are the pressure and temperature of the air in the mass balance room, respectively, and $u(m')$ refers to the uncertainty of the mass measurements for the tubes on the balance. If the trap is also used, the mass uncertainty contributions from the tubes and from escaped water are negligible compared with the trap uncertainty contributions, and for this case

$$\frac{u(m_{\text{w}})^2}{m_{\text{w}}^2} = \frac{2\rho_{\text{a}}^2 [V_{\text{t}} - V_{\text{s}}]^2}{m_{\text{w}}^2}$$
$$\times \left[\frac{u(P_{\text{a}})^2}{P_{\text{a}}^2} + \frac{u(T_{\text{a}})^2}{T_{\text{a}}^2} + \left(\frac{1}{\rho_{\text{a}}} \frac{d\rho_{\text{a}}}{d(\text{RH})} \right)^2 u(\text{RH})^2 \right]$$
$$+ \frac{5 u(m')^2}{m_{\text{w}}^2} + \frac{u(m_{\text{sens}})^2}{m_{\text{w}}^2}, \quad (12)$$

where V_{t} and V_{s} refer to the volumes of the trap and mass standard, respectively, m_{sens} is the mass of the sensitivity standard used with the trap and $u(m')$ refers to the mass-measurement uncertainty of the balance used for weighing the trap.

The uncertainty for the gas mass is given by

$$\frac{u(m_{\text{g}})^2}{m_{\text{g}}^2} = \frac{u(A)^2}{A^2} + \frac{u(\Delta z)^2}{h^2} + \frac{u(P_{\text{g}})^2}{P_{\text{g}}^2} + \frac{u(T_{\text{g}})^2}{T_{\text{g}}^2}, \quad (13)$$

where

$$u(\Delta z)^2 = u(z_1)^2 + u(z_2)^2. \quad (14)$$

Figure 9. Total expanded uncertainty ($k = 2$) for the gravimetric hygrometer as a function of (a) mass ratio and of (b) atmospheric-pressure dew/frost point. The curve labelled T_{g} is the uncertainty contribution from the gas temperature and m_{esc} is the contribution from the mass of the water that escapes the desiccant tubes.

Standard uncertainty components are listed in table 1 and plots of the total uncertainty as functions of mass ratio and of atmospheric-pressure dew point are shown in figure 9. The analysis yields a total expanded relative uncertainty of

$U \approx 0.09\%$ for $r > 250\,\mu g\,g^{-1}$ (atmospheric-pressure dew point greater than $-30\,^\circ C$).

For $r > 250\,\mu g\,g^{-1}$, measurement uncertainty for the water mass comes mainly from the uncertainty of the value of the sensitivity mass standard and from four subcomponent measurement uncertainties: tube/trap mass, air pressure, air temperature and air relative humidity. The measurement uncertainties are all type A uncertainties, as the type B uncertainties are cancelled out due to the measurement method. For $r \leqslant 250\,\mu g\,g^{-1}$, the water-mass uncertainty due to water escaping the collection is significant and becomes dominant as r decreases (see figure 9).

The uncertainty of the gas mass measurement is dominated by the gas temperature measurement uncertainties. These are not due to temperature measurement uncertainties of the SPRTs, which are less than $0.005\,^\circ C$, but rather from temperature non-uniformities inside the prover tubes. These temperature non-uniformities exist because of imperfect insulation from temperature non-uniformities in the room. The problem is exacerbated because each SPRT is located at the bottom of its prover tube rather than in a location where the temperature is closer to the average gas temperature in the tube, such as the centre. Unfortunately, it is logistically impossible to locate the SPRT in the centre of the prover tube, because it would interfere with the motion of the piston. Based on measurements of temperature non-uniformities outside the prover tubes under optimal thermal conditions (minimal heat loads in the room), we estimate the standard uncertainty of the temperature of the gas in the prover tubes under these conditions to be $0.1\,^\circ C$. The prover-tube gas temperature uncertainties are larger when significant heat loads exist in the room.

The next most significant uncertainty is from the gas pressure measurement, where the dominant uncertainty components are pressure gauge stability and calibration. The uncertainties of the prover-tube piston displacement and the prover-tube areas are also significant.

For $r \leqslant 250\,\mu g\,g^{-1}$, the total measurement uncertainty of r with the gravimetric hygrometer is dominated by uncertainty of the water mass escaping the collection tubes. For $r > 250\,\mu g\,g^{-1}$, the total uncertainty is dominated by the uncertainty of the temperature of the gas in the prover tubes. The next largest contributions come from the pressure of the gas in the prover tubes and the mass-measurement uncertainties for the water-collection tubes and trap.

5. Comparison with the NIST HHG

We have performed comparisons between the humidity measured by the NIST gravimetric hygrometer and that generated by NIST thermodynamic generators. Comparisons using the NIST Low Frost-point Generator [3] have been previously published [15]. Here we present comparison results using air humidified by the NIST HHG [1, 2, 16] in the two-pressure mode. The uncertainty budget for the HHG is described in [16]. The results of the comparison are shown in figure 10, which plots $\Delta r/r$, where $\Delta r \equiv r_{GH} - r_{HHG}$; here, r_{GH} is the mass ratio measured by the gravimetric hygrometer
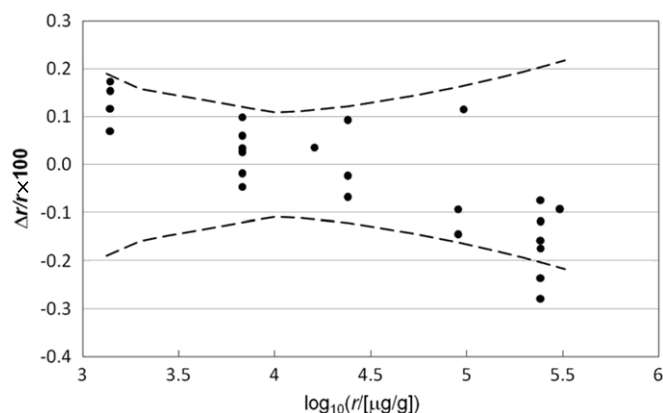

Figure 10. Comparison of mass ratio r measured by the gravimetric hygrometer with that generated by the NIST HHG, as a function of r. Here, $\Delta r \equiv r_{GH} - r_{HHG}$, where r_{GH} is the mass ratio measured by the gravimetric hygrometer and r_{HHG} is that generated using the HHG. The combined expanded ($k = 2$) relative uncertainties of the hygrometer and generator are represented by the dashed lines.

and r_{HHG} is that generated using the HHG. The range shown here corresponds to dew/frost points ranging from $-12\,^\circ C$ to $71\,^\circ C$. Here, the saturator pressure used was usually $\approx 200\,kPa$ and always was above $170\,kPa$.

Because of a non-optimal thermal environment in the laboratory where the comparisons were performed, we have increased the expanded uncertainty for the gravimetric hygrometer for these comparisons from those shown in figure 9. The non-optimal environment was due to the close proximity (1 m) of the HHG to the gravimetric hygrometer. Based on temperature-gradient measurements performed with differential thermocouples, we estimate that the standard uncertainty of the temperature of the gas increased from $u(T_g) = 0.1\,^\circ C$ when the HHG saturator temperature T_{sat} was $23\,^\circ C$ to $0.25\,^\circ C$ when T_{sat} was $85\,^\circ C$ and to $0.15\,^\circ C$ when T_{sat} was $0.5\,^\circ C$. Ideally it is not necessary to subject the gravimetric hygrometer to such large temperature non-uniformities (e.g. it could be operated in an adjacent room), and so in figure 9 we have used the value of $u(T_g)$ estimated for operating in a laboratory without these non-uniformities.

We estimate the expanded uncertainty ($k = 2$) of the mass ratio measurements by the gravimetric hygrometer to be between 0.09% and 0.20% over the range of humidity in the plot. The combined expanded relative uncertainty of the HHG and gravimetric hygrometer is shown in the figure as dotted lines and is estimated to be between 0.10% and 0.23% for all measurements in the plot. The values of $\Delta r/r$ are all within 0.3% and the averages of the points taken at one value of r are all within the combined uncertainties.

In the plot, the average values of $\Delta r/r$ clearly decrease with $\log_{10}(r/[\mu g\,g^{-1}])$. We suspect that this is due to systematic errors in the measurement of T_g due to the temperature non-uniformities in the prover tubes. Figure 11 shows a plot of the values of $\Delta r/r$ as a function of the operating temperature of the HHG, T_{HHG}. Note that the agreement is best when the HHG is operated at $20\,^\circ C$ and $40\,^\circ C$; at these values of T_{HHG} the room-temperature non-uniformities are relatively small.
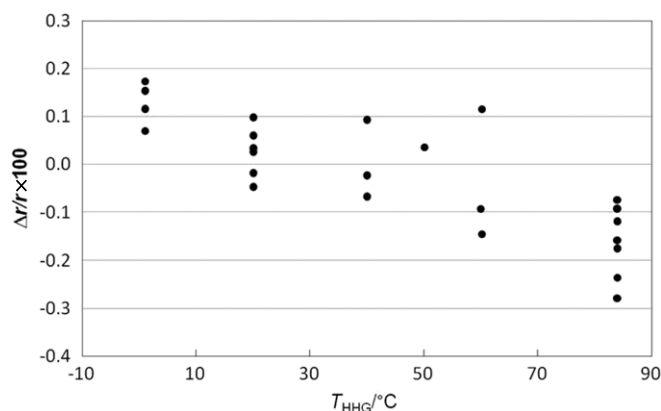
Figure 11. Plot of the values of $\Delta r/r$ shown in figure 9, as a function of T_{HHG}, the operating temperature of the HHG.

6. Conclusion

A new gravimetric hygrometer has been constructed as a primary humidity standard at NIST. This hygrometer employs a computer-automated continuous-flow gas-collection system, which makes use of the hygrometer much more convenient and also makes it possible to measure considerably lower humidity values. When used in an optimal thermal environment (i.e. minimal temperature gradients), the expanded relative uncertainty ($k = 2$) of values of r measured by the hygrometer is less than 0.16% for mass ratios of $r \geqslant 100\,\mu g\,g^{-1}$ and approximately 0.09% for $r \geqslant 250\,\mu g\,g^{-1}$. The dominant uncertainty elements for measurements of r are the gas temperature and pressure in the prover tubes, which are used for calculating the mass of the collected gas. For $r < 250\,\mu g\,g^{-1}$ the dominant uncertainty element is that of the water mass escaping the water-collection tubes, which causes the expanded uncertainty for r to increase beyond 1% for $r < 10\,\mu g\,g^{-1}$. The hygrometer is now operational, and comparisons have been made with the three NIST humidity generators currently in use. In the comparisons against the NIST hybrid generator, determinations of the generated mass ratios agreed with the gravimetric hygrometer measurements to within the combined measurement uncertainties, although the uncertainties of the hygrometer had to be increased to take into account the large temperature non-uniformities in the laboratory. With improved insulation of the enclosure containing the prover tubes and improved methods for determining the average gas temperature in the tubes, it may be possible to significantly lower the total uncertainty of the hygrometer measurements for $r \geqslant 250\,\mu g\,g^{-1}$. With better determination of the water mass escaping the water-collection tubes, it may also be possible to significantly lower the total uncertainty for $r < 250\,\mu g\,g^{-1}$.

Appendix A. Derivation of the uncertainty equation for the gravimetric hygrometer

Appendix A.1. General relations

The total uncertainty of a quantity z is related to the n individual uncertainty components y_i through the general law of error propagation [14]:

$$u(z)^2 = \sum_{i=1}^{n} \left(\frac{\partial z}{\partial y_i}\right) u(y_i)^2$$

$$+ 2\sum_{i=1}^{n-1}\sum_{j=i+1}^{n} r_{i,j}\frac{\partial z}{\partial y_i}\frac{\partial z}{\partial y_j} u(y_i)u(y_j). \tag{A1}$$

The relevant quantities and the derivatives $\partial z/\partial y_i$ may be found by expanding the differential $\mathrm{d}z$:

$$\mathrm{d}z = \sum_{i=1}^{n}\frac{\partial z}{\partial y_i}\mathrm{d}y_i. \tag{A2}$$

Performing this operation for the mass ratio using equation (1),

$$\mathrm{d}r = \frac{1}{m_g}\mathrm{d}m_w - \frac{m_w}{m_g^2}\mathrm{d}m_g \tag{A3}$$

or

$$\frac{\mathrm{d}r}{r} = \frac{\mathrm{d}m_w}{m_w} - \frac{\mathrm{d}m_g}{m_g}, \tag{A4}$$

yielding the relative uncertainty

$$\frac{u(r)^2}{r^2} = \frac{u(m_w)^2}{m_w^2} + \frac{u(m_g)^2}{m_g^2}. \tag{A5}$$

Appendix A.2. Uncertainty of the water mass

We first focus on the first term on the rhs of equation (A4) for a given water-collection tube. Differentiating equation (3),

$$\frac{\mathrm{d}m_w}{m_w} = \frac{1}{m_w}\left[\mathrm{d}m_t^f - \mathrm{d}m_t^i - \mathrm{d}(\Delta m_{tg})\right], \tag{A6}$$

where m_t is the tube mass and the superscripts 'i' and 'f' refer to the initial (before water collection) and final (after water collection) states, respectively. Also, Δm_{tg} refers to the change in the gas mass inside the tube from the initial to final state. Because $\mathrm{d}m_t^f$ and $\mathrm{d}m_t^i$ are correlated, the relative uncertainty is

$$\frac{u(m_w)^2}{m_w^2} = \frac{1}{m_w^2}\left[u(m_t^f - m_t^i)^2 + u(\Delta m_{tg})^2\right]. \tag{A7}$$

Appendix A.2.1. Mass increase of the water-collection tubes and water trap. The equation for the tube (or trap) mass is given by equation (2):

$$m_t = m_s + \rho_a(V_t - V_s) + (m_t' - m_s')$$
$$\times (m_{sens} - \rho_a V_{sens})/m_{sens}', \tag{A8}$$

where m_s is the real mass of the standard, m_{sens} is the real mass of the sensitivity standard, m_t' is the measured mass of the tube, m_s' is the measured mass of the standard and m_{sens}' is

the measured mass of the sensitivity standard. Differentiating equation (A8)

$$\mathrm{d}m_{\mathrm{t}} = \mathrm{d}m_{\mathrm{s}} + (V_{\mathrm{t}} - V_{\mathrm{s}})\,\mathrm{d}\rho_{\mathrm{a}} + \rho_{\mathrm{a}}\,(\mathrm{d}V_{\mathrm{t}} - \mathrm{d}V_{\mathrm{s}})$$
$$+ \frac{(m_{\mathrm{sens}} - \rho_{\mathrm{a}}V_{\mathrm{sens}})}{m'_{\mathrm{sens}}}\left(\mathrm{d}m'_{\mathrm{t}} - \mathrm{d}m'_{\mathrm{s}}\right)$$
$$+ \left(m'_{\mathrm{t}} - m'_{\mathrm{s}}\right)\left(\frac{\mathrm{d}m_{\mathrm{sens}}}{m'_{\mathrm{sens}}} - \frac{(m_{\mathrm{sens}} - \rho_{\mathrm{a}}V_{\mathrm{sens}})}{m'^{2}_{\mathrm{sens}}}\mathrm{d}m'_{\mathrm{sens}}\right)$$
$$- \frac{\rho_{\mathrm{a}}\mathrm{d}V_{\mathrm{sens}}}{m'_{\mathrm{sens}}} - \frac{V_{\mathrm{sens}}}{m'_{\mathrm{sens}}}\mathrm{d}\rho_{\mathrm{a}}\bigg). \tag{A9}$$

Equation (A9) may be simplified by recognizing that because the densities of the sensitivity weight, standard weight and tube are much greater than that of air, $(m_{\mathrm{sens}} - \rho_{\mathrm{a}}V_{\mathrm{sens}})/m'_{\mathrm{sens}} \cong 1$, $m'_{\mathrm{sens}} \cong m_{\mathrm{sens}}$, $m'_{\mathrm{s}} \cong m_{\mathrm{s}}$ and $m'_{\mathrm{t}} \cong m_{\mathrm{t}}$, yielding

$$\mathrm{d}m_{\mathrm{t}} = \mathrm{d}m_{\mathrm{s}} + (V_{\mathrm{t}} - V_{\mathrm{s}})\,\mathrm{d}\rho_{\mathrm{a}} + \rho_{\mathrm{a}}\,(\mathrm{d}V_{\mathrm{t}} - \mathrm{d}V_{\mathrm{s}}) + \mathrm{d}m'_{\mathrm{t}} - \mathrm{d}m'_{\mathrm{s}}$$
$$+ \frac{(m_{\mathrm{t}} - m_{\mathrm{s}})}{m_{\mathrm{sens}}}\left(\mathrm{d}m_{\mathrm{sens}} - \mathrm{d}m'_{\mathrm{sens}} - \rho_{\mathrm{a}}\mathrm{d}V_{\mathrm{sens}} - V_{\mathrm{sens}}\mathrm{d}\rho_{\mathrm{a}}\right). \tag{A10}$$

The air density differential may be expanded into its components:

$$\frac{\mathrm{d}\rho_{\mathrm{a}}}{\rho_{\mathrm{a}}} = \frac{1}{\rho_{\mathrm{a}}}\left(\frac{\mathrm{d}\rho_{\mathrm{a}}}{\mathrm{d}P}\mathrm{d}P + \frac{\mathrm{d}\rho_{\mathrm{a}}}{\mathrm{d}T}\mathrm{d}T + \frac{\mathrm{d}\rho_{\mathrm{a}}}{\mathrm{d}(\mathrm{RH})}\mathrm{d}(\mathrm{RH})\right)$$
$$\cong \left(\frac{\mathrm{d}P}{P} - \frac{\mathrm{d}T}{T} + \frac{1}{\rho_{\mathrm{a}}}\frac{\mathrm{d}\rho_{\mathrm{a}}}{\mathrm{d}(\mathrm{RH})}\mathrm{d}(\mathrm{RH})\right), \tag{A11}$$

where T is the absolute temperature. Inserting equation (A11) into equation (A10) gives

$$\mathrm{d}m_{\mathrm{t}} = \mathrm{d}m_{\mathrm{s}} + \rho_{\mathrm{a}}\left[V_{\mathrm{t}} - V_{\mathrm{s}} - \frac{(m_{\mathrm{t}} - m_{\mathrm{s}})}{m_{\mathrm{sens}}}V_{\mathrm{sens}}\right]$$
$$\times \left(\frac{\mathrm{d}P}{P} - \frac{\mathrm{d}T}{T} + \frac{1}{\rho_{\mathrm{a}}}\frac{\mathrm{d}\rho_{\mathrm{a}}}{\mathrm{d}(\mathrm{RH})}\mathrm{d}(\mathrm{RH})\right)$$
$$+ \rho_{\mathrm{a}}\,(\mathrm{d}V_{\mathrm{t}} - \mathrm{d}V_{\mathrm{s}}) + \mathrm{d}m'_{\mathrm{t}} - \mathrm{d}m'_{\mathrm{s}}$$
$$+ \frac{(m_{\mathrm{t}} - m_{\mathrm{s}})}{m_{\mathrm{sens}}}\left(\mathrm{d}m_{\mathrm{sens}} - \mathrm{d}m'_{\mathrm{sens}} - \rho_{\mathrm{a}}\mathrm{d}V_{\mathrm{sens}}\right). \tag{A12}$$

Using equation (A12) to subtract $\mathrm{d}m_{\mathrm{t}}^{\mathrm{i}}$ from $\mathrm{d}m_{\mathrm{t}}^{\mathrm{f}}$, and noting that $m_{\mathrm{s}}^{\mathrm{f}} = m_{\mathrm{s}}^{\mathrm{i}}$ and $m_{\mathrm{sens}}^{\mathrm{f}} = m_{\mathrm{sens}}^{\mathrm{i}}$,

$$\mathrm{d}m_{\mathrm{t}}^{\mathrm{f}} - \mathrm{d}m_{\mathrm{t}}^{\mathrm{i}} = \rho_{\mathrm{a}}^{\mathrm{f}}\left[V_{\mathrm{t}} - V_{\mathrm{s}} - \frac{(m_{\mathrm{t}}^{\mathrm{f}} - m_{\mathrm{s}})}{m_{\mathrm{sens}}}V_{\mathrm{sens}}\right]$$
$$\times \left[\frac{\mathrm{d}P^{\mathrm{f}}}{P^{\mathrm{f}}} - \frac{\mathrm{d}T^{\mathrm{f}}}{T^{\mathrm{f}}} + \frac{1}{\rho_{\mathrm{a}}^{\mathrm{f}}}\frac{\mathrm{d}\rho_{\mathrm{a}}^{\mathrm{f}}}{\mathrm{d}(\mathrm{RH})^{\mathrm{f}}}\mathrm{d}(\mathrm{RH})^{\mathrm{f}}\right]$$
$$- \rho_{\mathrm{a}}^{\mathrm{i}}\left[V_{\mathrm{t}} - V_{\mathrm{s}} - \frac{(m_{\mathrm{t}} - m_{\mathrm{s}})}{m_{\mathrm{sens}}}V_{\mathrm{sens}}\right]$$
$$\times \left[\frac{\mathrm{d}P^{\mathrm{i}}}{P^{\mathrm{i}}} - \frac{\mathrm{d}T^{\mathrm{i}}}{T^{\mathrm{i}}} + \frac{1}{\rho_{\mathrm{a}}^{\mathrm{i}}}\frac{\mathrm{d}\rho_{\mathrm{a}}^{\mathrm{i}}}{\mathrm{d}(\mathrm{RH})^{\mathrm{i}}}\mathrm{d}(\mathrm{RH})^{\mathrm{i}}\right] + \mathrm{d}m'^{\mathrm{f}}_{\mathrm{t}} - \mathrm{d}m'^{\mathrm{f}}_{\mathrm{s}}$$
$$- \mathrm{d}m'^{\mathrm{i}}_{\mathrm{t}} + \mathrm{d}m'^{\mathrm{i}}_{\mathrm{s}} + (\rho_{\mathrm{a}}^{\mathrm{f}} - \rho_{\mathrm{a}}^{\mathrm{i}})(\mathrm{d}V_{\mathrm{t}} - \mathrm{d}V_{\mathrm{s}})$$
$$+ \frac{(m_{\mathrm{t}}^{\mathrm{f}} - m_{\mathrm{t}}^{\mathrm{i}})}{m_{\mathrm{sens}}}\mathrm{d}m_{\mathrm{sens}} - \frac{(m_{\mathrm{t}}^{\mathrm{f}} - m_{\mathrm{s}})}{m_{\mathrm{sens}}}\mathrm{d}m'^{\mathrm{f}}_{\mathrm{sens}}$$
$$+ \frac{(m_{\mathrm{t}}^{\mathrm{i}} - m_{\mathrm{s}})}{m_{\mathrm{sens}}}\mathrm{d}m'^{\mathrm{i}}_{\mathrm{sens}} + \left[\frac{(m_{\mathrm{t}}^{\mathrm{f}} - m_{\mathrm{s}})}{m_{\mathrm{sens}}}\rho_{\mathrm{a}}^{\mathrm{f}} - \frac{(m_{\mathrm{t}}^{\mathrm{i}} - m_{\mathrm{s}})}{m_{\mathrm{sens}}}\rho_{\mathrm{a}}^{\mathrm{i}}\right]\mathrm{d}V_{\mathrm{sens}}. \tag{A13}$$

For the ith tube, let $m_{ti}^{\mathrm{i}} \equiv m_{\mathrm{t}}^{\mathrm{i}}$ and $m_{ti}^{\mathrm{f}} \equiv m_{\mathrm{t}}^{\mathrm{f}}$. For the weighings, m_{sens} is chosen such that for the first water-collection tube $m_{\mathrm{sens}} \cong m_{\mathrm{t1}}^{\mathrm{f}} - m_{\mathrm{t1}}^{\mathrm{i}}$ and m_{s} is chosen such that $m_{\mathrm{s}} \cong m_{\mathrm{t1}}^{\mathrm{i}}$. For the second and third water-collection tubes, m_{sens} is the same as that used for the first tube, but for these tubes $m_{\mathrm{t}}^{\mathrm{f}} \cong m_{\mathrm{t}}^{\mathrm{i}}$ since virtually all the water is collected in the first tube. Noting this, and that $V_{\mathrm{sens}} \ll V_{\mathrm{t}}$, we may simplify (A13):

$$\mathrm{d}m_{\mathrm{t}}^{\mathrm{f}} - \mathrm{d}m_{\mathrm{t}}^{\mathrm{i}} = \rho_{\mathrm{a}}^{\mathrm{f}}[V_{\mathrm{t}} - V_{\mathrm{s}}] \cdot \left[\frac{\mathrm{d}P^{\mathrm{f}}}{P^{\mathrm{f}}} - \frac{\mathrm{d}T^{\mathrm{f}}}{T^{\mathrm{f}}}\right.$$
$$\left. + \frac{1}{\rho_{\mathrm{a}}^{\mathrm{f}}}\frac{\mathrm{d}\rho_{\mathrm{a}}^{\mathrm{f}}}{\mathrm{d}(\mathrm{RH})^{\mathrm{f}}}\mathrm{d}(\mathrm{RH})^{\mathrm{f}}\right] - \rho_{\mathrm{a}}^{\mathrm{i}}[V_{\mathrm{t}} - V_{\mathrm{s}}]$$
$$\times \left[\frac{\mathrm{d}P^{\mathrm{i}}}{P^{\mathrm{i}}} - \frac{\mathrm{d}T^{\mathrm{i}}}{T^{\mathrm{i}}} + \frac{1}{\rho_{\mathrm{a}}^{\mathrm{i}}}\frac{\mathrm{d}\rho_{\mathrm{a}}^{\mathrm{i}}}{\mathrm{d}(\mathrm{RH})^{\mathrm{i}}}\mathrm{d}(\mathrm{RH})^{\mathrm{i}}\right] + \mathrm{d}m'^{\mathrm{f}}_{\mathrm{t}} - \mathrm{d}m'^{\mathrm{f}}_{\mathrm{s}}$$
$$- \mathrm{d}m'^{\mathrm{i}}_{\mathrm{t}} + \mathrm{d}m'^{\mathrm{i}}_{\mathrm{s}} + \left(\rho_{\mathrm{a}}^{\mathrm{f}} - \rho_{\mathrm{a}}^{\mathrm{i}}\right)(\mathrm{d}V_{\mathrm{t}} - \mathrm{d}V_{\mathrm{s}}) + \frac{(m_{\mathrm{t}}^{\mathrm{f}} - m_{\mathrm{t}}^{\mathrm{i}})}{m_{\mathrm{sens}}}\mathrm{d}m_{\mathrm{sens}}$$
$$- \frac{(m_{\mathrm{t}}^{\mathrm{f}} - m_{\mathrm{s}})}{m_{\mathrm{sens}}}\mathrm{d}m'^{\mathrm{f}}_{\mathrm{sens}} + \rho_{\mathrm{a}}^{\mathrm{f}}\mathrm{d}V_{\mathrm{sens}}. \tag{A14}$$

The first two tubes were weighed together in one measurement set, so their pressure and temperature uncertainties are correlated, as well as the uncertainties of $m_{\mathrm{s}}^{\mathrm{i}}$, $m_{\mathrm{s}}^{\mathrm{f}}$ and $m_{\mathrm{sens}}^{\mathrm{f}}$, since the same measurements are used for both tubes. For the first two tubes, equation (A14) becomes

$$\mathrm{d}m_{\mathrm{t1}}^{\mathrm{f}} - \mathrm{d}m_{\mathrm{t1}}^{\mathrm{i}} + \mathrm{d}m_{\mathrm{t2}}^{\mathrm{f}} - \mathrm{d}m_{\mathrm{t2}}^{\mathrm{i}} = 2\rho_{\mathrm{a}}^{\mathrm{f}}[V_{\mathrm{t}} - V_{\mathrm{s}}]$$
$$\times \left[\frac{\mathrm{d}P^{\mathrm{f}}}{P^{\mathrm{f}}} - \frac{\mathrm{d}T^{\mathrm{f}}}{T^{\mathrm{f}}} + \frac{1}{\rho_{\mathrm{a}}^{\mathrm{f}}}\frac{\mathrm{d}\rho_{\mathrm{a}}^{\mathrm{f}}}{\mathrm{d}(\mathrm{RH})^{\mathrm{f}}}\mathrm{d}(\mathrm{RH})^{\mathrm{f}}\right]$$
$$- 2\rho_{\mathrm{a}}^{\mathrm{i}}[V_{\mathrm{t}} - V_{\mathrm{s}}] \cdot \left[\frac{\mathrm{d}P^{\mathrm{i}}}{P^{\mathrm{i}}} - \frac{\mathrm{d}T^{\mathrm{i}}}{T^{\mathrm{i}}} + \frac{1}{\rho_{\mathrm{a}}^{\mathrm{i}}}\frac{\mathrm{d}\rho_{\mathrm{a}}^{\mathrm{i}}}{\mathrm{d}(\mathrm{RH})^{\mathrm{i}}}\mathrm{d}(\mathrm{RH})^{\mathrm{i}}\right]$$
$$+ \mathrm{d}m'^{\mathrm{f}}_{\mathrm{t1}} - \mathrm{d}m'^{\mathrm{i}}_{\mathrm{t1}} + \mathrm{d}m'^{\mathrm{f}}_{\mathrm{t2}} - \mathrm{d}m'^{\mathrm{i}}_{\mathrm{t2}} - 2\mathrm{d}m'^{\mathrm{f}}_{\mathrm{s}} + 2\mathrm{d}m'^{\mathrm{i}}_{\mathrm{s}} - \mathrm{d}m'^{\mathrm{f}}_{\mathrm{sens}}$$
$$+ \mathrm{d}m_{\mathrm{sens}} + \rho_{\mathrm{a}}^{\mathrm{f}}\mathrm{d}V_{\mathrm{sens}} + \left(\rho_{\mathrm{a}}^{\mathrm{f}} - \rho_{\mathrm{a}}^{\mathrm{i}}\right)(\mathrm{d}V_{\mathrm{t}} - \mathrm{d}V_{\mathrm{s}}). \tag{A15}$$

For the third tube, separate measurements were made for pressure, temperature, $m_{\mathrm{s}}^{\mathrm{i}}$, $m_{\mathrm{s}}^{\mathrm{f}}$ and $m_{\mathrm{sens}}^{\mathrm{f}}$, so these are uncorrelated with those for the first two tubes. For this tube, equation (A14) simplifies to

$$\mathrm{d}m_{\mathrm{t3}}^{\mathrm{f}} - \mathrm{d}m_{\mathrm{t3}}^{\mathrm{i}} = \rho_{\mathrm{a}}^{\mathrm{f}}[V_{\mathrm{t}} - V_{\mathrm{s}}]$$
$$\times \left[\frac{\mathrm{d}P^{\mathrm{f}}}{P^{\mathrm{f}}} - \frac{\mathrm{d}T^{\mathrm{f}}}{T^{\mathrm{f}}} + \frac{1}{\rho_{\mathrm{a}}^{\mathrm{f}}}\frac{\mathrm{d}\rho_{\mathrm{a}}^{\mathrm{f}}}{\mathrm{d}(\mathrm{RH})^{\mathrm{f}}}\mathrm{d}(\mathrm{RH})^{\mathrm{f}}\right]$$
$$- \rho_{\mathrm{a}}^{\mathrm{i}}[V_{\mathrm{t}} - V_{\mathrm{s}}] \cdot \left[\frac{\mathrm{d}P^{\mathrm{i}}}{P^{\mathrm{i}}} - \frac{\mathrm{d}T^{\mathrm{i}}}{T^{\mathrm{i}}} + \frac{1}{\rho_{\mathrm{a}}^{\mathrm{i}}}\frac{\mathrm{d}\rho_{\mathrm{a}}^{\mathrm{i}}}{\mathrm{d}(\mathrm{RH})^{\mathrm{i}}}\mathrm{d}(\mathrm{RH})^{\mathrm{i}}\right] + \mathrm{d}m'^{\mathrm{f}}_{\mathrm{t3}}$$
$$- \mathrm{d}m'^{\mathrm{f}}_{\mathrm{s}} - \mathrm{d}m'^{\mathrm{i}}_{\mathrm{t3}} + \mathrm{d}m'^{\mathrm{i}}_{\mathrm{s}} + \left(\rho_{\mathrm{a}}^{\mathrm{f}} - \rho_{\mathrm{a}}^{\mathrm{i}}\right)(\mathrm{d}V_{\mathrm{t}} - \mathrm{d}V_{\mathrm{s}}) + \rho_{\mathrm{a}}^{\mathrm{f}}\mathrm{d}V_{\mathrm{sens}}. \tag{A16}$$

For the first and second tubes, the uncertainty for $m_{t1}^f - m_{t1}^i + m_{t2}^f - m_{t2}^i$ is then given by

$$u(m_{t1}^f - m_{t1}^i + m_{t2}^f - m_{t2}^i)^2 = 4\rho_a^{f2}[V_t - V_s]^2$$
$$\times \left[\frac{u(P^f)^2}{(P^f)^2} + \frac{u(T^f)^2}{(T^f)^2} + \left(\frac{1}{\rho_a^f}\frac{d\rho_a^f}{d(RH^f)}\right)^2 u(RH^f)^2\right]$$
$$+ 4\rho_a^{i2}[V_t - V_s]^2 \cdot \left[\frac{u(P^i)^2}{(P^i)^2} + \frac{u(T^i)^2}{(T^i)^2}\right.$$
$$\left. + \left(\frac{1}{\rho_a^i}\frac{d\rho_a^i}{d(RH^i)}\right)^2 u(RH^i)^2\right] + u(m_{t1}'^f)^2 + u(m_{t1}'^i)^2$$
$$+ u(m_{t2}'^f)^2 + u(m_{t2}'^i)^2 + 4u(m_s'^f)^2 + 4u(m_s'^i)^2$$
$$+ u(m_{sens}'^f)^2 + u(m_{sens}')^2 + (\rho_a^f - \rho_a^i)^2 \left[u(V_t)^2 + u(V_s)^2\right]$$
$$+ \rho_a^{f2} u(V_{sens})^2. \tag{A17}$$

And for the third tube,

$$u(m_{t3}^f - m_{t3}^i)^2 = \rho_a^{f2}[V_t - V_s]^2 \cdot \left[\frac{u(P^f)^2}{(P^f)^2} + \frac{u(T^f)^2}{(T^f)^2}\right.$$
$$\left. + \left(\frac{1}{\rho_a^f}\frac{d\rho_a^f}{d(RH^f)}\right)^2 u(RH^f)^2\right] + \rho_a^{i2}[V_t - V_s]^2$$
$$\times \left[\frac{u(P^i)^2}{(P^i)^2} + \frac{u(T^i)^2}{(T^i)^2} + \left(\frac{1}{\rho_a^i}\frac{d\rho_a^i}{d(RH^i)}\right)^2 u(RH^i)^2\right]$$
$$+ u(m_{t3}'^f)^2 + u(m_{t3}'^i)^2 + u(m_s'^f)^2 + u(m_s'^i)^2$$
$$+ (\rho_a^f - \rho_a^i)^2 \left[u(V_t)^2 + u(V_s)^2\right] + \rho_a^{f2} u(V_{sens})^2. \tag{A18}$$

In equations (A17) and (A18), the uncertainties for the pressure, temperature, relative humidity and mass are all type A uncertainties, as all the type B uncertainties are correlated and have been subtracted out. We also note that these random uncertainties are all identical for a given type of measurement; hence

$$u(P^f) = u(P^i) \equiv u(P),$$

$$u(T^f) = u(T^i) \equiv u(T),$$

$$u(RH^f) = u(RH^i) \equiv u(RH),$$

$$u(m_{ti}'^f) = u(m_{ti}'^i) = u(m_s'^f) = u(m_s'^i) = u(m_{sens}'^f)$$
$$= u(m_{sens}'^i) \equiv u(m'). \tag{A19}$$

Then, noting that

$$P^f \cong P^i \equiv P,$$
$$T^f \cong T^i \equiv T, \tag{A20}$$
$$\rho_a^f \cong \rho_a^i \equiv \rho_a.$$

Equation (A17) simplifies to

$$u(m_{t1}^f - m_{t1}^i + m_{t2}^f - m_{t2}^i)^2 = 8\rho_a^2[V_t - V_s]^2$$
$$\times \left[\frac{u(P)^2}{(P)^2} + \frac{u(T)^2}{(T)^2} + \left(\frac{1}{\rho_a}\frac{d\rho_a}{d(RH)}\right)^2 u(RH)^2\right]$$
$$+ 13u(m')^2 + u(m_{sens})^2 + \left(\rho_a^f - \rho_a^i\right)^2 \left[u(V_t)^2 + u(V_s)^2\right]$$
$$+ \rho_a^{f2} u(V_{sens})^2 \tag{A21}$$

and equation (A18) simplifies to

$$u(m_{t3}^f - m_{t3}^i)^2 = 2\rho_a^2[V_t - V_s]^2$$
$$\times \left[\frac{u(P)^2}{(P)^2} + \frac{u(T)^2}{(T)^2} + \left(\frac{1}{\rho_a}\frac{d\rho_a}{d(RH)}\right)^2 u(RH)^2\right] + 4u(m')^2$$
$$+ \left(\rho_a^f - \rho_a^i\right)^2 \left[u(V_t)^2 + u(V_s)^2\right] + \rho_a^{f2} u(V_{sens})^2. \tag{A22}$$

We can simplify equations (A21) and (A22) further by neglecting the insignificant uncertainties. The uncertainty contributions from the pressure and temperature measurements, each mass measurement and the sensitivity mass are typically $100\,\mu g$, $70\,\mu g$ and $120\,\mu g$, respectively. By contrast, assuming a 1% difference between ρ_a^f and ρ_a^i, the contributions from the uncertainties of V_t and V_s are $10\,\mu g$. Assuming the volume of the 2 g sensitivity standard is known to 1%, the contribution from the uncertainty of V_{sens} is $3\,\mu g$. We may therefore consider the uncertainties from V_t, V_s and V_{sens} to be negligible. The total mass-difference uncertainty for the three tubes is then

$$u_{tot}(m_t^f - m_t^i)^2$$
$$= u(m_{t1}^f - m_{t1}^i + m_{t2}^f - m_{t2}^i)^2 + u(m_{t3}^f - m_{t3}^i)^2$$
$$= 10\rho_a^2[V_t - V_s]^2 \cdot \left[\frac{u(P)^2}{P^2} + \frac{u(T)^2}{T^2}\right.$$
$$\left. + \left(\frac{1}{\rho_a}\frac{d\rho_a}{d(RH)}\right)^2 u(RH)^2\right] + 17u(m')^2 + u(m_{sens}).$$
$$\tag{A23}$$

If the water trap is used along with the three water-collection tubes, the uncertainty contributions from the water trap are much larger than those from the water-collection tubes, and so the latter contributions may be neglected. The mass-difference differential is then given by (A14), where the subscript 't' refers to the trap and the subscripts 's' and 'sens' refer to the mass standard and sensitivity mass for the trap. Once again, m_{sens} is chosen such that $m_{sens} \cong m_t^f - m_t^i$ and m_s is chosen such that $m_s \cong m_t^i$. Considering the uncertainty contributions from V_t, V_s and V_{sens} to be negligible, equation (A14) becomes

$$dm_t^f - dm_t^i = \rho_a^f[V_t - V_s] \cdot \left[\frac{dP^f}{P^f} - \frac{dT^f}{T^f}\right.$$
$$\left. + \frac{1}{\rho_a^f}\frac{d\rho_a^f}{d(RH)^f}d(RH)^f\right] - \rho_a^i[V_t - V_s]$$
$$\times \left[\frac{dP^i}{P^i} - \frac{dT^i}{T^i} + \frac{1}{\rho_a^i}\frac{d\rho_a^i}{d(RH)^i}d(RH)^f\right]$$
$$+ dm_t'^f - dm_s'^f - dm_t'^i + dm_s'^i + dm_{sens}'^f + dm_{sens}. \tag{A24}$$

Using equation (A20), the uncertainty is then

$$u(m_t^f - m_t^i)^2 = 2\rho_a^2 [V_t - V_s]^2$$

$$\times \left[\frac{u(P)^2}{P^2} + \frac{u(T)^2}{T^2} + \left(\frac{1}{\rho_a} \frac{d\rho_a}{d(RH)} \right)^2 u(RH)^2 \right]$$

$$+ 5u(m')^2 + u(m_{sens}), \tag{A25}$$

where $u(m')$ refers to the mass-measurement uncertainty of the balance used for weighing the trap.

Appendix A.2.2. Mass decrease of gas in a water-collection tube (or water trap). From equation (3),

$$\Delta m_{tg} = V_g^f \rho_{tg}^f - V_g^i \rho_{tg}^i. \tag{A26}$$

Differentiating equation (A26) and assuming $\rho_{tg}^f \cong \rho_{tg}^i$,

$$d(\Delta m_{tg}) = V_{tg}^f d\rho_{tg}^f + \rho_{tg}^f dV_{tg}^f - V_g^i d\rho_{tg}^i - \rho_{tg}^i dV_{tg}^i$$

$$= V_{tg}^f d\rho_{tg}^f - V_{tg}^i d\rho_{tg}^i + \rho_{tg}^f d(V_{tg}^f - V_{tg}^i). \tag{A27}$$

Here, (see equation (3) and equation (6))

$$V_{tg}^f - V_{tg}^i = \chi m_w, \tag{A28}$$

where the volume χ taken up by the collected water is given by

$$\chi = 0.819 \, \text{cm}^3 \, \text{g}^{-1} \, \text{(water-collection tubes)},$$

$$\chi = 1/\rho_w \, \text{(water trap)}.$$

Differentiating equation (A28) and inserting it in equation (A27) gives

$$d(\Delta m_{tg}) = V_{tg}^f d\rho_{tg}^f - V_{tg}^i d\rho_{tg}^i + \rho_{tg}^f (\chi dm_w + m_w d\chi). \tag{A29}$$

Using the relationship of equation (A11) (with no humidity),

$$d(\Delta m_{tg}) = V_{tg}^f \rho_{tg}^f \left(\frac{dP_{tg}^f}{P_{tg}^f} - \frac{dT_{tg}^f}{T_{tg}^f} \right) - V_{tg}^i \rho_{tg}^i \left(\frac{dP_{tg}^i}{P_{tg}^i} - \frac{dT_{tg}^i}{T_{tg}^i} \right)$$

$$+ \rho_{tg}^f (\chi dm_w + m_w d\chi). \tag{A30}$$

The uncertainty is then given by

$$u(\Delta m_{tg})^2 = (V_{tg}^f \rho_{tg}^f)^2 \left(\frac{u(P_{tg}^f)^2}{P_{tg}^{f2}} + \frac{u(T_{tg}^f)^2}{T_{tg}^{f2}} \right)$$

$$+ (V_{tg}^i \rho_{tg}^i)^2 \left(\frac{u(P_{tg}^i)^2}{P_{tg}^{i2}} + \frac{u(T_{tg}^i)^2}{T_{tg}^{i2}} \right)$$

$$+ (\rho_{tg}^f)^2 [\chi^2 u(m_w)^2 + m_w^2 u(\chi)^2]. \tag{A31}$$

Recognizing that

$$P_{tg}^f \cong P_{tg}^i \equiv P_{tg},$$

$$T_{tg}^f \cong T_{tg}^i \equiv T_{tg},$$

$$\rho_{tg}^f \cong \rho_{tg}^i \equiv \rho_{tg}, \tag{A32}$$

$$u(P_{tg}^f) \cong u(P_{tg}^i) \equiv u(P_{tg}),$$

$$u(T_{tg}^f) \cong u(T_{tg}^i) \equiv u(T_{tg}),$$

equation (A31) may be approximated as

$$u(\Delta m_{tg})^2 = \rho_{tg}^2 \left([V_{tg}^{i2} + V_{tg}^{f2}] \cdot \left[\frac{u(P_{tg})^2}{P_{tg}^2} + \frac{u(T_{tg})^2}{T_{tg}^2} \right] \right.$$

$$\left. + [\chi^2 u(m_w)^2 + m_w^2 u(\chi)^2] \right). \tag{A33}$$

The quantitative value of this uncertainty is typically about $u(\Delta m_{tg})/m_w \cong 5 \times 10^{-5}$, which is negligible compared with other uncertainties.

Appendix A.3. Uncertainty of the gas mass

The collected gas mass is given by equation (9):

$$m_g = \rho_g^f V_g + \left(\rho_g^f - \rho_g^i \right) V_d. \tag{A34}$$

Differentiating equation (A34),

$$dm_g = \rho_g^f dV_g + (V_g + V_d) d\rho_g^f + \left(\rho_g^f - \rho_g^i \right) dV_d - V_d d\rho_g^i. \tag{A35}$$

Using equation (8) and the approximation of equation (A11) for a gas with no humidity,

$$dm_g = \rho_g^f V_g \left(\frac{dA}{A} + \frac{dz_2}{h} - \frac{dz_1}{h} \right)$$

$$+ (V_g + V_d) \rho_g^f \left(\frac{dP_g^f}{P_g^f} - \frac{dT_g^f}{T_g^f} \right)$$

$$+ \left(\rho_g^f - \rho_g^f \right) dV_d - V_d \rho_g^i \left(\frac{dP_g^i}{P_g^i} - \frac{dT_g^i}{T_g^i} \right). \tag{A36}$$

Recognizing that $\rho_g^f \cong \rho_g^i$ and $m_g \cong \rho_g^f V_g$, equation (A36) becomes

$$\frac{dm_g}{m_g} = \left(\frac{dA}{A} + \frac{dz_2}{h} - \frac{dz_1}{h} \right) + \left(1 + \frac{V_d}{V_g} \right) \left(\frac{dP_g^f}{P_g^f} - \frac{dT_g^f}{T_g^f} \right)$$

$$- \frac{V_d}{V_g} \left(\frac{dP_g^i}{P_g^i} - \frac{dT_g^i}{T_g^i} \right). \tag{A37}$$

The gas mass uncertainty is then

$$\frac{u(m_g)^2}{m_g^2} = \left(\frac{u(A)^2}{A^2} + \frac{u(z_2)^2}{h^2} + \frac{u(z_1)^2}{h^2} \right)$$

$$+ \left(1 + \frac{V_d}{V_g} \right)^2 \left(\frac{u(P_g^f)^2}{P_g^{f2}} + \frac{u(T_g^f)^2}{T_g^{f2}} \right)$$

$$+ \left(\frac{V_d}{V_g} \right)^2 \left(\frac{u(P_g^i)^2}{P_g^{i2}} + \frac{u(T_g^i)^2}{T_g^{i2}} \right). \tag{A38}$$

Since

$$u(P_g^f) \cong u(P_g^i) \equiv u(P_g),$$

$$u(T_g^f) \cong u(T_g^i) \equiv u(T_g),$$

$$P_g^f \cong P_g^i \equiv P_g, \tag{A39}$$

$$T_g^f \cong T_g^i \equiv T_g,$$

$$V_g \gg V_d.$$

We may then approximate

$$\frac{u(m_\mathrm{g})^2}{m_\mathrm{g}^2} = \frac{u(A)^2}{A^2} + \frac{u(\Delta z)^2}{h^2} + \frac{u(P_\mathrm{g})^2}{P_\mathrm{g}^2} + \frac{u(T_\mathrm{g})^2}{T_\mathrm{g}^2}, \qquad (A40)$$

where

$$\Delta z = z_2 - z_1 \qquad (A41)$$

and

$$u\left(\Delta z\right)^2 = u\left(z_1\right)^2 + u\left(z_2\right)^2. \qquad (A42)$$

References

[1] Scace G E, Meyer C W, Miller W W and Hodges J T 2007 An overview of the NIST Hybrid Humidity Generator *Proc. 5th Int. Symp. on Humidity and Moisture (Rio de Janeiro)* (Rio de Janeiro, Brazil: INMETRO)

[2] Meyer C W, Miller W W, Ripple D C and Scace G E 2008 *Int. J. Thermophys.* **29** 1606–14

[3] Scace G E and Hodges J T 2001 *Proc. TEMPMEKO 2001: 8th Int. Symp. on Temperature and Thermal Measurements in Industry and Science (Berlin, Germany)* ed B Fellmuth and J Seidel pp 597–602

[4] Regnault V 1845 *Ann. Chim. Phys. Ser. 3* **15** 129–236

[5] Shaw W N 1888 *Phil. Trans. R. Soc. Lond.* A **179** 73–149

[6] Scholz G 1984 *Bull. OIML* **97** 18–27

[7] Bell S A 1998 *Papers and Abstracts from the 3rd Int. Symp. on Humidity and Moisture (Teddington, UK)* (Teddington, UK: National Physical Laboratory) pp 20–7

[8] Wexler A 1948 *J. Res. NBS* **40** 479–86

[9] Wexler A and Hyland R W 1963 The NBS standard hygrometer *NBS Monograph* 73

[10] Picard A, Davis R S, Glaser M and Fujii K 2008 *Metrologia* **45** 149–55

[11] Ciddor P E 1996 *Appl. Opt.* **35** 1566–73

[12] Wexler A and Hyland R W 1983 *ASHRAE Trans. Part IIa* **89** 520–35

[13] McLinden M O and Losch-Will C 2007 *J. Chem. Thermodyn.* **39** 507–30

[14] ISO 1993 *Guide to the Expression of Uncertainty in Measurement* (Geneva: International Organization for Standardization) (updated as JCGM 100:2008 available at http://www.bipm.org/en/publications/guides/gum.html)

[15] Meyer C W, Hodges J T, Hyland R W, Scace G E, Valencia-Rodriguez J and Whetstone J R 2007 Automated continuous-flow gravimetric hygrometer as a primary humidity standard *Proc. 5th Int. Symp. on Humidity and Moisture* (Rio de Janeiro, Brazil: INMETRO)

[16] Meyer C W, Hodges J T, Huang PH, Miller W W, Ripple D C and Scace G E 2008 *Calibration of Hygrometers with the Hybrid Humidity Generator* NIST Special Publication 250–83